

See discussions, stats, and author profiles for this publication at: <https://www.researchgate.net/publication/11628073>

[1,2,4]Triazino[4,3-a]benzimidazole acetic acid derivatives: a new class of selective aldose reductase inhibitors.

ARTICLE *in* JOURNAL OF MEDICINAL CHEMISTRY · JANUARY 2002

Impact Factor: 5.45 · Source: PubMed

CITATIONS

11

READS

14

10 AUTHORS, INCLUDING:



Concettina La Motta

Università di Pisa

105 PUBLICATIONS 1,307 CITATIONS

SEE PROFILE



Sabrina Taliani

Università di Pisa

92 PUBLICATIONS 1,022 CITATIONS

SEE PROFILE



Ettore Novellino

University of Naples Federico II

610 PUBLICATIONS 8,828 CITATIONS

SEE PROFILE



Antonio Lavecchia

University of Naples Federico II

118 PUBLICATIONS 2,415 CITATIONS

SEE PROFILE

[1,2,4]Triazino[4,3-*a*]benzimidazole Acetic Acid Derivatives: A New Class of Selective Aldose Reductase Inhibitors

Federico Da Settimo,^{*,†} Giampaolo Primofiore,[†] Antonio Da Settimo,[†] Concettina La Motta,[†] Sabrina Taliani,[†] Francesca Simorini,[†] Ettore Novellino,[‡] Giovanni Greco,[‡] Antonio Lavecchia,[‡] and Enrico Boldrini[§]

Dipartimento di Scienze Farmaceutiche, Università di Pisa, Via Bonanno 6, 56126 Pisa, Italy, Dipartimento di Chimica Farmaceutica e Tossicologica, Università di Napoli "Federico II", Via Domenico Montesano, 49, 80131 Napoli, Italy, and Farmigea S.p.A., Via Carmignani 2, 56127, Pisa, Italy

Received May 8, 2001

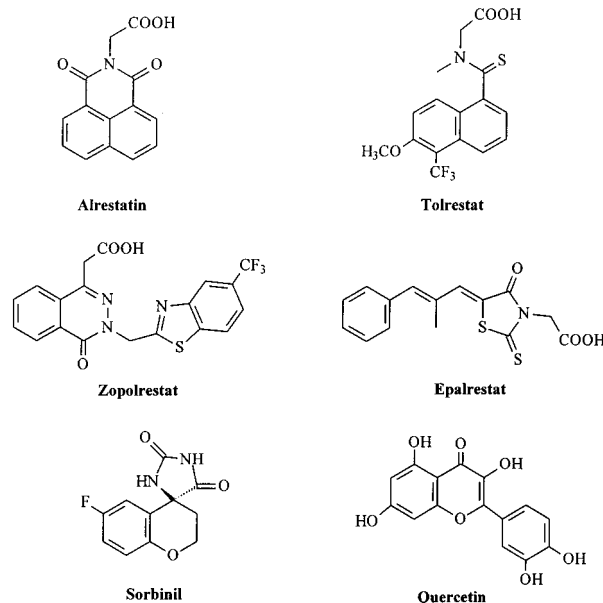
Acetic acid derivatives of [1,2,4]triazino[4,3-*a*]benzimidazole (TBI) were synthesized and tested in vitro and in vivo as a novel class of aldose reductase (ALR2) inhibitors. Compound **3**, (10-benzyl[1,2,4]triazino[4,3-*a*]benzimidazol-3,4(10*H*)-dion-2-yl)acetic acid, displayed the highest inhibitory activity ($IC_{50} = 0.36 \mu M$) and was found to be effective in preventing cataract development in severely galactosemic rats when administered as an eyedrop solution. All the compounds investigated were selective for ALR2, since none of them inhibited appreciably aldehyde reductase, sorbitol dehydrogenase, or glutathione reductase. The activity of **3** was lowered by inserting various substituents on the pendant phenyl ring, by shifting the acetic acid moiety from the 2 to the 3 position of the TBI nucleus, or by cleaving the TBI system to yield benzimidazolylidenehydrazines as open-chain analogues. A three-dimensional model of human ALR2 was built, taking into account the conformational changes induced by the binding of inhibitors such as zopolrestat, to simulate the docking of **3** into the enzyme active site. The theoretical binding mode of **3** was fully consistent with the structure–activity relationships in the TBI series and will guide the design of novel ALR2 inhibitors.

Introduction

Despite recent advances in the chemistry and molecular pharmacology of antidiabetic drugs, diabetes still remains a life-threatening disease. Tissues capable of insulin-independent glucose uptake develop structural and functional damage (retinopathy, nephropathy, cataract, keratopathy, neuropathy, and angiopathy) in more than 50% of diabetics. A strict glycemic control prevents or at least delays the onset of such complications. However, because close control is difficult to maintain and because there is a parallel risk of severe hypoglycemia and obesity in intensive insulin-treated patients, considerable efforts have been made to find novel, effective antidiabetic agents acting by mechanisms independent of the control of blood glucose.^{1–3}

Several experimental data have revealed a link between glucose metabolism via the polyol pathway and long-term diabetic complications. Aldose reductase (alditol/NADP⁺ oxidoreductase, EC 1.1.1.21, ALR2), the first enzyme of the pathway, catalyzes the NADPH-dependent reduction of glucose to sorbitol.^{2,4} Therefore, inhibition of ALR2 has become an attractive therapeutic strategy, and a large number of ALR2 inhibitors (ARIs) have been identified to date. Currently known ARIs can be divided into three classes: (i) acetic acid derivatives, including alrestatin, tolrestat, zopolrestat, and epalrestat; (ii) cyclic imides such as sorbinil; (iii) flavonoids, whose prototype is quercetin (Chart 1).⁵

Chart 1. Well-Known ALR2 Inhibitors



Structural requirements for ALR2 inhibitory activity are a planar cyclic moiety and an acidic function ionized at the ALR2 active site.^{6–9}

One of the most important requirements of clinically useful ARIs is ALR2 selectivity over closely related enzymes such as aldehyde reductase (ALR1), sorbitol dehydrogenase (SD), and glutathione reductase (GR). ALR1 belongs to the aldo–keto reductase family like ALR2 and exhibits the highest homology in structure (51% sequence identity) and activity with ALR2.¹⁰ SD is the second enzyme in the polyol pathway, and its

* To whom correspondence should be addressed. Phone: 39 50 500209. Fax: 39 50 40517. E-mail: fsettimo@farm.unipi.it.

[†] Università di Pisa.

[‡] Università "Federico II" di Napoli.

[§] Farmigea S.p.A.

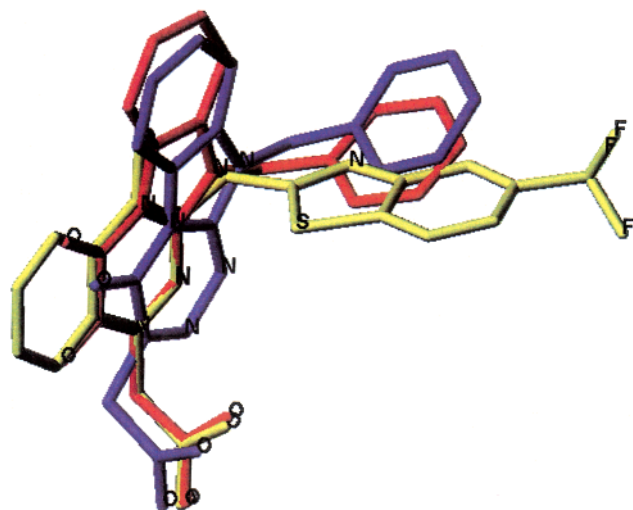


Figure 1. Overlay of **3** (red) and **25** (blue) on the experimentally determined ALR2-bound conformation of zopolrestat (yellow). The conformations of the TBI derivatives were selected and aligned as described in the Computational Chemistry part of the Experimental Section.

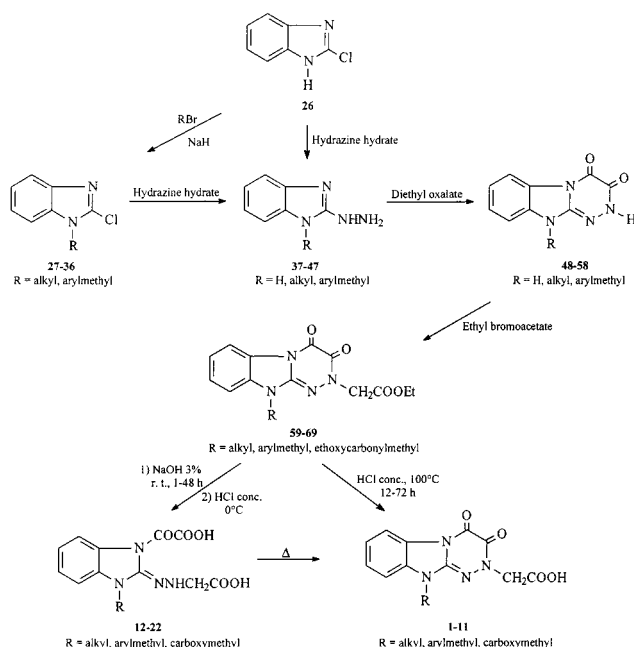
inhibition increases sorbitol levels, thus reducing the effects of ALR2 inhibition.¹¹ GR maintains physiological levels of glutathione, which in turn prevents glycosylation of cellular protein and protects against oxidative stress. The intracellular accumulation of oxidized glutathione, resulting from inhibition of GR, leads to a structural modification of ALR2 that reduces its sensitivity to ARI action.^{12,13}

In addition to problems related to selectivity among homologous enzymes, ARI-based therapy suffers from many limitations due to pharmacokinetic problems, reversibility of diabetic neuropathy, adverse reactions, and poor reproducibility of clinical measurements.¹⁴ Only epalrestat is on the Japanese market nowadays. For these reasons, there is still a need to identify and develop clinically effective and well-tolerated ARIs.

This paper describes the synthesis and the biological evaluation of novel ARIs featuring an acetic acid residue at the 2 or 3 position of the [1,2,4]triazino[4,3-*a*]benzimidazole (TBI) nucleus (compounds **1–11** or **23–25**, respectively). The TBI system proved to be a suitable scaffold for several compounds recently described by us as selective ligands at the benzodiazepine¹⁵ and A₁ adenosine¹⁶ receptors. An overlay of molecular models of **3** and **25** on the ALR2-bound conformation of zopolrestat⁶ gave support to our project because it showed a satisfactory match of the common acetic acid chain, the phthalazine/TBI systems and the benzothiazole/phenyl rings (Figure 1). To better delineate the structure–activity relationships (SARs) of this new class of ARIs, the benzimidazolylidenehydrazine (BIH) derivatives **12–22**, intermediates in the synthesis of **1–11**, were likewise tested.

Compound **3**, the most active ALR2 inhibitor among those examined, and its *i*-propyl ester **73** were also investigated in vivo for their ability to prevent cataract development in galactosemic rats. Finally, docking simulations of **3** into the ALR2 active site were carried out to rationalize the SARs observed and to guide, perspective, the design of new analogues.

Scheme 1



Chemistry

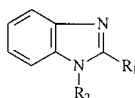
The title compounds **1–11** were synthesized as outlined in Scheme 1. The substituted 1-alkyl-2-chlorobenzimidazoles **27–36** (Table 1) were prepared in good yields from the commercially available 2-chlorobenzimidazole **26** by reaction with the appropriate alkyl halide in the presence of sodium hydride.¹⁷ Treatment of **26–36** with hydrazine hydrate¹⁸ resulted in the hydrazino derivatives **37–47** (Table 1), which were cyclized to the corresponding triazino-benzimidazoles **48–58** (Table 2) by refluxing with an equimolar amount of diethyl oxalate in ethanolic solution.¹⁹ Reaction of **48–58** with ethyl bromoacetate in refluxing acetone, in the presence of anhydrous potassium carbonate,¹¹ gave the ester derivatives **59–69** (Table 3). These were hydrolyzed by aqueous sodium hydroxide to give, after acidification, the dicarboxylic acids **12–22** (Table 4), which underwent thermal cyclization to the triazino-benzimidazole acetic acids **1–11** (Table 5). Alternatively, the target acids **1–11** could be obtained by hydrolysis of compounds **59–69** with concentrated hydrochloric acid at 100 °C.

The regioisomeric acetic acids **23–25** were prepared in accordance with the synthetic route shown in Scheme 2. Treatment of the hydrazino derivatives **37, 38**, and **40** with diethyl acetylenedicarboxylate in refluxing methanol²⁰ afforded the ethyl esters **70–72** (Table 6), which by hydrolysis with concentrated hydrochloric acid yielded the desired acids **23–25** (Table 6).

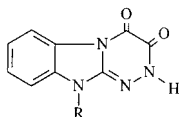
To improve the ocular bioavailability of carboxylic acid **3**, the more lipophilic *i*-propyl ester **73** was also prepared. Thus, a mixture of compound **51** with *i*-propyl bromoacetate was refluxed in acetone solution in the presence of anhydrous potassium carbonate to give the target ester **73** (see Experimental Section).

Biochemistry and Pharmacology

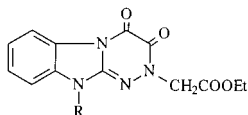
Compounds **1–25** were evaluated for their in vitro inhibitory activity against ALR2 as well as against ALR1, SD, and GR. Primary in vitro screening was

Table 1. Physical Properties of Benzimidazole Derivatives **30**, **31**, **34**–**36**, **38**, **39**, **41**–**47**

no.	R ₁	R ₂	yield (%)	recryst solv	mp (°C)	formula ^a
30	Cl	CH ₂ C ₆ H ₄ –4-CH ₃	85	petroleum ether 60–80	119–120	C ₁₅ H ₁₃ ClN ₂
31	Cl	CH ₂ C ₆ H ₄ –4-OCH ₃	85	AcOEt	96–97	C ₁₅ H ₁₃ ClN ₂ O
34	Cl	CH ₂ C ₆ H ₄ –4-CF ₃	64	petroleum ether 60–80	84–85	C ₁₅ H ₁₀ ClF ₃ N ₂
35	Cl	CH ₂ C ₆ H ₃ –3,4-F ₂	74	petroleum ether 60–80	88–89	C ₁₄ H ₉ ClF ₂ N ₂
36	Cl	CH ₂ C ₆ H ₃ –2-F–4-Br	97	EtOH	106–107	C ₁₄ H ₉ BrClFN ₂
38	NHNH ₂	CH ₃	91	H ₂ O	148–151	C ₈ H ₁₀ N ₄
39	NHNH ₂	CH ₂ CH ₂ CH ₃	99	H ₂ O	108–111	C ₁₀ H ₁₄ N ₄
41	NHNH ₂	CH ₂ C ₆ H ₄ –4-CH ₃	56	H ₂ O	86–89	C ₁₅ H ₁₆ N ₄
42	NHNH ₂	CH ₂ C ₆ H ₄ –4-OCH ₃	96	toluene	83–86	C ₁₅ H ₁₆ N ₄ O
43	NHNH ₂	CH ₂ C ₆ H ₄ –4-Cl	70	H ₂ O	193–198 (dec)	C ₁₄ H ₁₃ ClN ₄
44	NHNH ₂	CH ₂ C ₆ H ₄ –4-F	67	H ₂ O	138–151 (dec)	C ₁₄ H ₁₃ FN ₄
45	NHNH ₂	CH ₂ C ₆ H ₄ –4-CF ₃	88	H ₂ O	156–160	C ₁₅ H ₁₃ F ₃ N ₄
46	NHNH ₂	CH ₂ C ₆ H ₃ –3,4-F ₂	90	<i>i</i> -PrOH	108–111	C ₁₄ H ₁₂ F ₂ N ₄
47	NHNH ₂	CH ₂ C ₆ H ₃ –2-F–4-Br	85	EtOH	116–120	C ₁₄ H ₁₂ BrFN ₄

^a Elemental analyses for C, H, N were within ±0.4% of the calculated values.**Table 2.** Physical Properties of 10-Alkyl[1,2,4]triazino[4,3-*a*]benzimidazol-3,4(10*H*)-dione Derivatives **49**–**58**

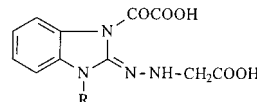
no.	R	yield (%)	recryst solv	mp (°C)	formula ^a
49	CH ₃	53	DMF	>300	C ₁₀ H ₈ N ₄ O ₂
50	CH ₂ CH ₂ CH ₃	66	DMF	294–295	C ₁₂ H ₁₂ N ₄ O ₂
51	CH ₂ C ₆ H ₅	74	DMF	>300	C ₁₆ H ₁₂ N ₄ O ₂
52	CH ₂ C ₆ H ₄ –4-CH ₃	62	DMF	>300	C ₁₇ H ₁₄ N ₄ O ₂
53	CH ₂ C ₆ H ₄ –4-OCH ₃	46	DMF	>300	C ₁₇ H ₁₄ N ₄ O ₃
54	CH ₂ C ₆ H ₄ –4-Cl	42	DMF	>300	C ₁₆ H ₁₁ ClN ₄ O ₂
55	CH ₂ C ₆ H ₄ –4-F	33	DMF	278–280	C ₁₆ H ₁₁ FN ₄ O ₂
56	CH ₂ C ₆ H ₄ –4-CF ₃	31	DMF	296–298	C ₁₇ H ₁₁ F ₃ N ₄ O ₂
57	CH ₂ C ₆ H ₃ –3,4-F ₂	81	DMF	210–212	C ₁₆ H ₁₀ F ₂ N ₄ O ₂
58	CH ₂ C ₆ H ₃ –2-F–4-Br	54	DMF	278–280	C ₁₆ H ₁₀ BrFN ₄ O ₂

^a Elemental analyses for C, H, N were within ±0.4% of the calculated values.**Table 3.** Physical Properties of Ethyl (10-Alkyl[1,2,4]triazino[4,3-*a*]benzimidazol-3,4(10*H*)-dion-2-yl)acetate Derivatives **59**–**69**

no.	R	yield (%)	recryst solv	mp (°C)	formula ^a
59	CH ₃	74	EtOH	208–209	C ₁₄ H ₁₄ N ₄ O ₄
60	CH ₂ CH ₂ CH ₃	90	EtOH	168–169	C ₁₆ H ₁₈ N ₄ O ₄
61	CH ₂ C ₆ H ₅	57	EtOH	211–213	C ₂₀ H ₁₈ N ₄ O ₄
62	CH ₂ C ₆ H ₄ –4-CH ₃	70	EtOH	195–196	C ₂₁ H ₂₀ N ₄ O ₄
63	CH ₂ C ₆ H ₄ –4-OCH ₃	90	EtOH	177–178	C ₂₁ H ₂₀ N ₄ O ₅
64	CH ₂ C ₆ H ₄ –4-Cl	73	EtOH	218–220	C ₂₀ H ₁₇ ClN ₄ O ₄
65	CH ₂ C ₆ H ₄ –4-F	71	AcOEt	222–223	C ₂₀ H ₁₇ FN ₄ O ₄
66	CH ₂ C ₆ H ₄ –4-CF ₃	63	EtOH	243–246	C ₂₁ H ₁₇ F ₃ N ₄ O ₄
67	CH ₂ C ₆ H ₃ –3,4-F ₂	75	EtOH	182–183	C ₂₀ H ₁₆ F ₂ N ₄ O ₄
68	CH ₂ C ₆ H ₃ –2-F–4-Br	59	EtOH	206–209	C ₂₀ H ₁₆ BrFN ₄ O ₄
69	CH ₂ COOEt	39	EtOH	202–203	C ₁₇ H ₁₈ N ₄ O ₄

^a Elemental analyses for C, H, N were within ±0.4% of the calculated values.

conducted on a water-soluble enzymatic extract purified from rat lenses.^{21–24} IC₅₀ values were determined by linear regression analysis of the log of the concentration–response curve. Compounds **1**–**25** were also as-

Table 4. Physical Properties of (1-Substituted-3-oxalo-1*H*,3*H*-benzimidazol-2-ylidenehydrazino)acetic Acids **12**–**22**

no.	R	yield (%)	recryst solv	cycliz temp ^a (°C)	formula ^b
12	CH ₃	62	H ₂ O	231–235	C ₁₂ H ₁₂ N ₄ O ₅
13	CH ₂ CH ₂ CH ₃	95	H ₂ O	167–168	C ₁₄ H ₁₆ N ₄ O ₅
14	CH ₂ C ₆ H ₅	85	H ₂ O	238–250	C ₁₈ H ₁₆ N ₄ O ₅
15	CH ₂ C ₆ H ₄ –4-CH ₃	64	H ₂ O	205–215	C ₁₉ H ₁₈ N ₄ O ₅
16	CH ₂ C ₆ H ₄ –4-OCH ₃	61	MeOH	193–196	C ₁₉ H ₁₈ N ₄ O ₆
17	CH ₂ C ₆ H ₄ –4-Cl	57	AcOEt	197–200	C ₁₈ H ₁₅ ClN ₄ O ₅
18	CH ₂ C ₆ H ₄ –4-F	44	H ₂ O	200–202	C ₁₈ H ₁₅ FN ₄ O ₅
19	CH ₂ C ₆ H ₄ –4-CF ₃	41	acetone	205–206	C ₁₉ H ₁₅ F ₃ N ₄ O ₅
20	CH ₂ C ₆ H ₃ –3,4-F ₂	76	AcOEt	215–216	C ₁₈ H ₁₄ F ₂ N ₄ O ₅
21	CH ₂ C ₆ H ₃ –2-F–4-Br	70	AcOEt	185–190	C ₁₈ H ₁₄ BrFN ₄ O ₅
22	CH ₂ COOH	77	H ₂ O	178–185	C ₁₃ H ₁₂ N ₄ O ₇

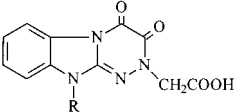
^a Temperature at which compounds cyclize to triazinobenzimidazole derivatives **1**–**11**. ^b Elemental analyses for C, H, N were within ±0.4% of the calculated values.

sayed for their ability to inhibit SD²⁵ and two other enzymes not involved in the polyol pathway, namely, ALR1²⁶ and GR.²⁷ Sorbinil,²⁸ tolrestat,^{29,30} and quercetin³¹ were used as the reference standards.

Compound **3** and its *i*-propyl ester **73** were investigated in vivo for their ability to prevent cataract development in severely galactosemic rats.²⁸ Their effectiveness was evaluated with respect to tolrestat as a highly potent reversible inhibitor of lenticular ALR2 when topically administered to rats fed with 50% galactose diet.³⁰

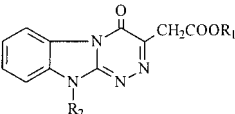
Results and Discussion

Biological Evaluation. Table 7 lists the inhibitory activities against ALR2 of compounds **1**–**25** expressed as IC₅₀ values. Several compounds (**6**, **7**, **9**, **10**, **14**, **19**, **20**, and **25**) exhibited IC₅₀ values in the low micromolar range. The TBI derivative **3** turned out the most potent inhibitor of the series, with an IC₅₀ value (0.36 μM) similar to that of sorbinil (0.65 μM) and 7-fold worse than that of tolrestat. The activity was lowered by inserting various substituents on the phenyl ring of **3** to yield **4**–**10**, as well as replacing the benzyl group of **3** with much less lipophilic substituents such as a

Table 5. Physical Properties of (10-Substituted[1,2,4]triazino[4,3-*a*]benzimidazol-3,4(10*H*)-dion-2-yl)acetic Acids **1–11**


no.	R	yield ^a (%)	recryst solv	mp (°C)	formula ^b
1	CH ₃	38 (39)	MeOH	> 300	C ₁₂ H ₁₀ N ₄ O ₄
2	CH ₂ CH ₂ CH ₃	75 (65)	EtOH	199–200	C ₁₄ H ₁₄ N ₄ O ₄
3	CH ₂ C ₆ H ₅	68 (63)	EtOH	252–255 (dec)	C ₁₈ H ₁₄ N ₄ O ₄
4	CH ₂ C ₆ H ₄ –4-CH ₃	73 (70)	EtOH	258–262 (dec)	C ₁₉ H ₁₆ N ₄ O ₄
5	CH ₂ C ₆ H ₄ –4-OCH ₃	61 (60)	EtOH	258–261	C ₁₉ H ₁₆ N ₄ O ₅
6	CH ₂ C ₆ H ₄ –4-Cl	85 (88)	EtOH	255–257 (dec)	C ₁₈ H ₁₃ ClN ₄ O ₄
7	CH ₂ C ₆ H ₄ –4-F	63 (60)	EtOH	250–253 (dec)	C ₁₈ H ₁₃ FN ₄ O ₄
8	CH ₂ C ₆ H ₄ –4-CF ₃	46 (48)	MeOH	240–246 (dec)	C ₁₉ H ₁₃ F ₃ N ₄ O ₄
9	CH ₂ C ₆ H ₃ –3,4-F ₂	71 (65)	EtOH	250–256 (dec)	C ₁₈ H ₁₂ F ₂ N ₄ O ₄
10	CH ₂ C ₆ H ₃ –2-F–4-Br	92 (90)	EtOH	262–266 (dec)	C ₁₈ H ₁₂ BrFN ₄ O ₄
11	CH ₂ COOH	53 (54)	EtOH	238–244 (dec)	C ₁₃ H ₁₀ N ₄ O ₆

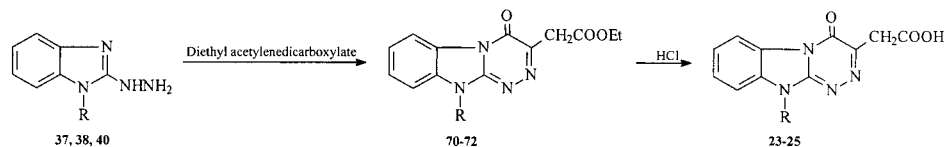
^a Thermal cyclization yield (method A). In parentheses ester hydrolysis yield (method B). ^b Elemental analyses for C, H, N were within ±0.4% of the calculated values.

Table 6. Physical Properties of ([1,2,4]Triazino[4,3-*a*]benzimidazol-4(10*H*)-on-3-yl)acetic Acid Derivatives **23–25** and **70–72**


no.	R ₁	R ₂	yield (%)	recryst solv	mp (°C)	formula ^a
70	CH ₂ CH ₃	H	75	toluene	237–238 (dec)	C ₁₃ H ₁₂ N ₄ O ₃
71	CH ₂ CH ₃	CH ₃	86	MeOH	195–198 (dec)	C ₁₄ H ₁₄ N ₄ O ₃
72	CH ₂ CH ₃	CH ₂ C ₆ H ₅	85	EtOH	161–164	C ₂₀ H ₁₈ N ₄ O ₃
23	H	H	95	AcOH	> 300	C ₁₁ H ₈ N ₄ O ₃
24	H	CH ₃	90	AcOH	230–231	C ₁₂ H ₁₀ N ₄ O ₃
25	H	CH ₂ C ₆ H ₅	92	AcOH	180–182	C ₁₈ H ₁₄ N ₄ O ₃

^a Elemental analyses for C, H, N were within ±0.4% of the calculated values.

Scheme 2



methyl (**1**), an *n*-propyl (**2**), or an acetic acid group (**11**). Taken together, these data suggest that a small-size hydrophobic pocket within the enzyme active site is available to the benzyl moiety of **3**. The BIH derivatives **12–22** were generally less active than their corresponding closed-chain analogues TBIs **1–11**, the only exception to this trend being the pair **19/8**. The higher flexibility of BIHs compared with their TBI counterparts may explain the difference in activity observed between the two series.

The shift of the acetic acid moiety from position 2 to position 3 of the TBI system, to give compounds **23–25**, was tolerated (compare **1** vs **24**) or detrimental (compare **3** vs **25**). Evidently, the TBI-2-acetic acids feature the best spatial relationship among the pharmacophoric groups.

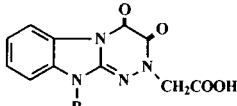
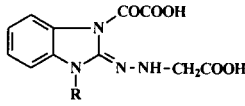
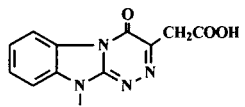
Finally, compounds **1–25** were all found to be selective inhibitors of ALR2 because none of them showed any appreciable inhibitory property toward ALR1, SD, and GR.

Pharmacological Evaluation of Compounds 3 and 73. Compound **3** was administered as an eyedrop solution in the precorneal region to investigate its *in vivo* ability to prevent cataract development in severely galactosemic rats. Topical administration can in prin-

ciple achieve significant drug levels in the lens with negligible effects on other tissues, thus avoiding bioavailability and/or metabolism-related problems associated with systemic administration.³⁰ It has been reported^{32–34} that esters of acid drugs display a better corneal permeability and ocular bioavailability by virtue of their higher lipophilicity. Considering that *i*-propyl esters have shown good permeability in the corneal tissue,³² the *i*-propyl ester **73** was prepared and tested *in vivo* as a prodrug of compound **3**. The pharmacological data are reported in Table 8. After 21 days of a 50% galactose diet, 90% of the animals treated only with vehicle developed nuclear cataract. Those treated with 3% ophthalmic solution of **3** and **73** and with 1% ophthalmic solution of tolrestat were protected by 50%, 60%, and 53%, respectively, whereas no nuclear cataracts were detected in rats that were administered a 3% ophthalmic solution of tolrestat. The similar fairly high potency displayed by **3** and its prodrug **73** suggests that **3** is already characterized by an optimal hydrophilic–lipophilic balance to permeate the cornea and that **73** is quickly hydrolyzed to the active acid by corneal esterases.

Molecular Modeling. To rationalize the SARs of the TBI derivatives at the molecular level and to perspec-

Table 7. ALR2 Inhibition Data of Acid Derivatives 1–25^a

no.	R	Aldose Reductase IC ₅₀ ^b (μM)
		
1	CH ₃	24.80 (17.41–32.24)
2	CH ₂ CH ₂ CH ₃	37.20 (31.22–44.33)
3	CH ₂ C ₆ H ₅	0.36 (0.25–0.45)
4	CH ₂ C ₆ H ₄ -4-CH ₃	13.30 (7.90–18.62)
5	CH ₂ C ₆ H ₄ -4-OCH ₃	42.60 (29.80–55.40)
6	CH ₂ C ₆ H ₄ -4-Cl	4.15 (2.69–6.59)
7	CH ₂ C ₆ H ₄ -4-F	4.58 (2.75–5.95)
8	CH ₂ C ₆ H ₄ -4-CF ₃	23.90 (15.84–32.07)
9	CH ₂ C ₆ H ₃ -3,4-F ₂	4.42 (2.46–6.96)
10	CH ₂ C ₆ H ₃ -2-F-4-Br	4.47 (3.82–5.23)
11	CH ₂ COOH	13.50 (8.01–18.55)
		
12	CH ₃	108.6 (76.02–141.2)
13	CH ₂ CH ₂ CH ₃	46.50 (37.24–57.60)
14	CH ₂ C ₆ H ₅	4.50 (2.95–6.89)
15	CH ₂ C ₆ H ₄ -4-CH ₃	45.90 (28.30–64.00)
16	CH ₂ C ₆ H ₄ -4-OCH ₃	44.50 (31.15–57.80)
17	CH ₂ C ₆ H ₄ -4-Cl	10.00 (6.28–13.11)
18	CH ₂ C ₆ H ₄ -4-F	14.80 (10.36–20.20)
19	CH ₂ C ₆ H ₄ -4-CF ₃	2.63 (1.95–3.41)
20	CH ₂ C ₆ H ₃ -3,4-F ₂	9.72 (6.99–12.60)
21	CH ₂ C ₆ H ₃ -2-F-4-Br	12.50 (8.75–16.25)
22	CH ₂ COOH	236.0 (141.5–330.0)
		
23	H	35.90 (25.13–46.67)
24	CH ₃	17.00 (11.90–22.10)
25	CH ₂ C ₆ H ₅	5.44 (3.80–6.50)
sorbinil		0.65 (0.49–0.82)
tolrestat		0.05 (0.03–0.06)
quercetin		7.81 (5.47–10.15)

^a All compounds did not inhibit ALR1, SD, and GR up to a concentration of 10^{−3} M. ^b IC₅₀ (95% CL) values represent the concentration required to produce 50% enzyme inhibition.

tively guide the design of novel ARIs, we developed a model of compound **3** bound to ALR2. The results of these studies are summarized here, whereas details are given in the Computational Chemistry part of the Experimental Section.

Crystal structures of ALR2 complexed with zopolrestat,⁶ tolrestat,⁷ sorbinil,⁷ and alrestatin⁸ clearly show that inhibitors bind at the catalytic site and induce significant conformational changes in a loop (residues 121–135) and a short segment (residues 298–303) to open and fill a contiguous hydrophobic pocket. This so-called specificity pocket, closed in the absence of the

Table 8. Effect of Treatment with Ophthalmic Solution of **3**, **73**, and Tolrestat on Development of Nuclear Cataract in Severely Galactosemic Rats

day of treatment	rats with nuclear cataract (%)				
	control	3 (3%)	73 (3%)	tolrestat (1%)	tolrestat (3%)
11	13	0	0	0	0
12	25	0	10	0	0
13	25	0	10	0	0
14	25	10	10	23	0
15	25	10	10	32	0
16	31	10	10	32	0
17	50	10	10	32	0
18	50	40	40	43	0
19	75	40	40	43	0
20	88	50	40	47	0
21	90	50	40	47	0

inhibitor, is a key determinant for selectivity, since it hosts hydrophobic moieties of ARIs that are more effective against ALR2 than ALR1. Although the three-dimensional structure of the human ALR2/NADP⁺/zopolrestat complex has been determined by Wilson et al.,⁶ only the corresponding coordinates of the C_α atoms have been filed in the Brookhaven Protein Data Bank³⁵ (PDB entry code 1MAR). To take into account the conformational switching undergone by ALR2 upon ARI binding, we built a model of human ALR2 starting from the crystal structures of the human ALR2 holoenzyme (PDB entry code 1ADS)³⁶ and the porcine ALR2/NADP⁺/tolrestat complex (PDB entry code 1AH3).⁷ Briefly, fragments 121–135 and 298–303 of human ALR2 (closed specificity pocket) were replaced with those of porcine ALR2 (open specificity pocket) and nonidentical side chains were mutated into those of the human type using the SYBYL/MUTATE command. The resulting protein model was geometry-optimized by molecular mechanics calculations using the AMBER force field.^{37,38}

Although the inhibition assays on our compounds were conducted on rat ALR2, the use of a model of human ALR2 for docking studies is justified by the following facts: (i) the crystal structure of rat ALR2 is unknown; (ii) the human and rat sequences of this enzyme are characterized by 81% of identity and 88% of homology;³⁹ (iii) all active-site residues, including those of the specificity pocket, are largely conserved across the ALR2 isoforms so far sequenced.

Representative energetically stable conformations of **3** were sought for docking calculations. For this purpose, we used the SYBYL/SEARCH module to scan the torsion angles τ_1 , τ_2 , τ_3 , and τ_4 defined in Figure 2. Low-energy conformations (those within 2 kcal/mol of the global minimum conformation) were then clustered into 16 families through the SYBYL/SPREADSHEET/FAMILY routine. The lowest energy member of each family was submitted to docking using the automated DOCK software package.^{40–43} This program estimates the likelihood of each generated binding mode by a scoring function based on a molecular mechanics force field. The geometry of the top scoring ALR2/NADP⁺/**3** complex was refined by extensive energy minimization and molecular dynamics simulations in a solvated system at room temperature. Interestingly, the best docking conformation of **3** yielded the most satisfactory overlay on the ALR2-bound conformation of zopolrestat (Figure 1).

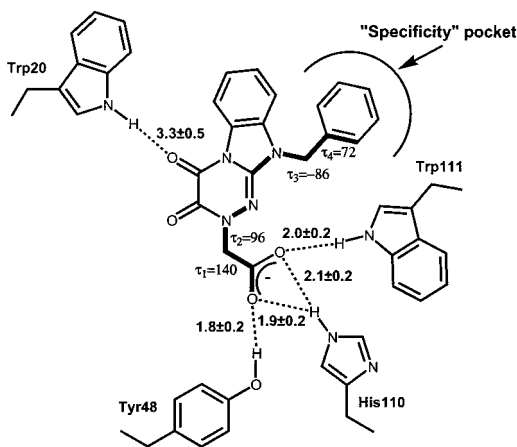


Figure 2. Scheme of the main interactions observed in the molecular dynamics simulation of the ALR2/NADP⁺/3 complex. Mean values of intermolecular hydrogen bond distances and of their standard deviations are given. The values of the torsion angles τ_1 , τ_2 , τ_3 , and τ_4 define the conformation of the inhibitor.

The main features of the final docking model are schematically represented in Figure 2. The three-dimensional structure of the ALR2/NADP⁺/3 complex is shown in Figure 3, where only the amino acids located within 5 Å of the inhibitor are displayed.

Throughout the entire molecular dynamics simulation, the carboxylate oxygens of **3** were anchored into the so-called anionic binding site via a network of hydrogen bonds involving Tyr48, His110, and Trp111 side chains. This suggests that the carboxylate group is an essential requirement for the inhibitory activity of **3** and its TBI derivatives. A further hydrogen bond between the carbonyl oxygen at the 4 position of the TBI system and the N^ε1 hydrogen of Trp20 was also found to contribute to complex stabilization, although it was observed to be frequently cleaved during the simulation, giving an average distance longer than that of an ideal hydrogen bond.

A hydrophobic cavity made up of the Trp20, Trp79, Phe122, and Trp219 side chains hosts the TBI nucleus of the inhibitor. The Phe122 side chain makes contact with the fused benzene and the benzyl moiety of **3** via a π -stacking and a T-shaped interaction, respectively.

The phenyl ring of **3** fits into the specificity pocket (the same one that hosts the zopolrestat benzothiazole moiety)⁶ made up of four aromatic residues (Trp79, Trp111, Phe115, Phe122), two aliphatic residues (Val130, Leu300), and five polar residues (Cys80, Thr113, Cys298, Ser302, Cys303). This specificity pocket does not appear to tolerate any further steric bulk, consistent with the detrimental effects exerted by substituents on the phenyl ring of **3**. Our model is not contradicted by the favorable effect of the trifluoromethyl group featured by the benzothiazole moiety of zopolrestat as well as by the fused-benzene system of tolrestat, both occupying the specificity pocket. In fact, the phenyl ring of **3** is not exactly coincident in space with either the benzothiazole or the fused-benzene moieties of zopolrestat and tolrestat (Figure 4). From a methodological point of view, it is worth noting that the pharmacophore-based (Figure 1) and the docking-based (Figure 4) alignments of **3** on zopolrestat are fairly similar.

Conclusions

We have presented acetic acid derivatives of the [1,2,4]triazino[4,3-*a*]benzimidazole (TBI) nucleus as a novel class of selective ARIs. Compound **3**, the most potent derivative of the series, exhibited an ALR2 inhibitory activity ($IC_{50} = 0.36 \mu M$) similar to that of sorbinil ($0.65 \mu M$) and proved to be effective in preventing cataract development in severely galactosemic rats when administered as an eyedrop solution. Docking simulations of **3** into a model of the ALR2 binding site were performed to explain SARs and to guide, perspective, the design of new analogues.

Experimental Section

1. Chemistry. Melting points were determined using a Reichert Köfeler hot-stage apparatus and are uncorrected. Infrared spectra were recorded with a PYE/UNICAM Infracord model PU 9516 spectrophotometer in Nujol mulls. Routine nuclear magnetic resonance spectra were recorded in DMSO-*d*₆ solution on a Varian CFT 20 spectrometer operating at 80 MHz, using tetramethylsilane (TMS) as the internal standard. Mass spectra were obtained on a Hewlett-Packard 5988 A spectrometer using a direct injection probe and an electron beam energy of 70 eV. Evaporations were made in vacuo (rotary evaporator). Analytical TLC was carried out on Merck 0.2 mm precoated silica gel aluminum sheets (60 F-254). Elemental analyses were performed by our analytical laboratory, and the results agreed with theoretical values to within $\pm 0.4\%$.

The alkyl halides 4-methylbenzyl chloride, 4-methoxybenzyl chloride, 4-(trifluoromethyl)benzyl chloride, 3,4-difluorobenzyl bromide, and 4-bromo-2-fluorobenzyl bromide used to obtain compounds **30**, **31**, **34**–**36**, respectively, and 2-chlorobenzimidazole, **26**, were from Sigma-Aldrich. The following compounds were prepared in accordance with reported procedures: 2-chloro-1-methylbenzimidazole, **27**, mp 114–116 °C (lit.⁴⁴ mp 107–113.5 °C); 2-chloro-1-*n*-propylbenzimidazole, **28**, bp 140–143 °C, 0.5 mmHg (lit.⁴⁴ bp 110.5–111.5 °C, 0.3 mmHg); 1-benzyl-2-chlorobenzimidazole, **29**, mp 108–109 °C (lit.⁴⁴ mp 108–111 °C); 1-(4-chlorobenzyl)-2-chlorobenzimidazole, **32**, mp 73–75 °C (lit.⁴⁵ mp 73–75 °C); 2-chloro-1-(4-fluorobenzyl)benzimidazole, **33**, mp 74–79 °C (lit.⁴⁶ mp 75–76 °C); 2-hydrazinobenzimidazole, **37**, mp 148–151 °C (lit.¹⁸ mp 146–147 °C); 1-benzyl-2-hydrazinobenzimidazole, **40**, mp 134–135 °C (lit.¹⁸ mp 140–145 °C); [1,2,4]triazino[4,3-*a*]benzimidazol-3,4-(10*H*)-dione **48**, mp >300 °C (lit.¹⁹ mp 360 °C).

General Procedure for the Synthesis of 1-Alkyl-2-chlorobenzimidazoles 30, 31, 34–36. Sodium hydride (1.2 mmol, 50% dispersion in mineral oil) was added portionwise, under a nitrogen atmosphere, to an ice-cooled solution of 2-chlorobenzimidazole (**26**, 0.153 g, 1 mmol) in 5 mL of freshly distilled DMF. Once hydrogen evolution had ceased, the appropriate alkyl halide (1.2 mmol) was added dropwise and the reaction mixture was maintained under stirring at room temperature until the disappearance of the starting material (2–18 h, TLC analysis). The solution was then slowly poured onto crushed ice, and the solid precipitate was collected, washed with water, and recrystallized. Yields, recrystallization solvents, and melting points of the products are reported in Table 1. Spectral data for **30**, which is representative of the title compounds, are listed below.

2-Chloro-1-(4-methylbenzyl)benzimidazole, 30. IR, ν cm⁻¹: 1450, 1360, 720. ¹H NMR, δ : 2.25 (s, 3H, CH₃), 5.44 (s, 2H, CH₂), 7.10–7.49 (m, 8H, ArH). MS, *m/e*: 256 [M⁺], 105, base.

General Procedure for the Synthesis of 1-Alkyl-2-hydrazinobenzimidazoles 38, 39, 41–47. The appropriate 1-alkyl-2-chlorobenzimidazole (**27**, **28**, **30**–**36**, 1 mmol) was heated at 160 °C in a Pyrex capped tube with 0.1 mL of hydrazine hydrate for 5 h. After the mixture was cooled, a white solid separated, which was collected and recrystallized. Yields, recrystallization solvents, and melting points of the

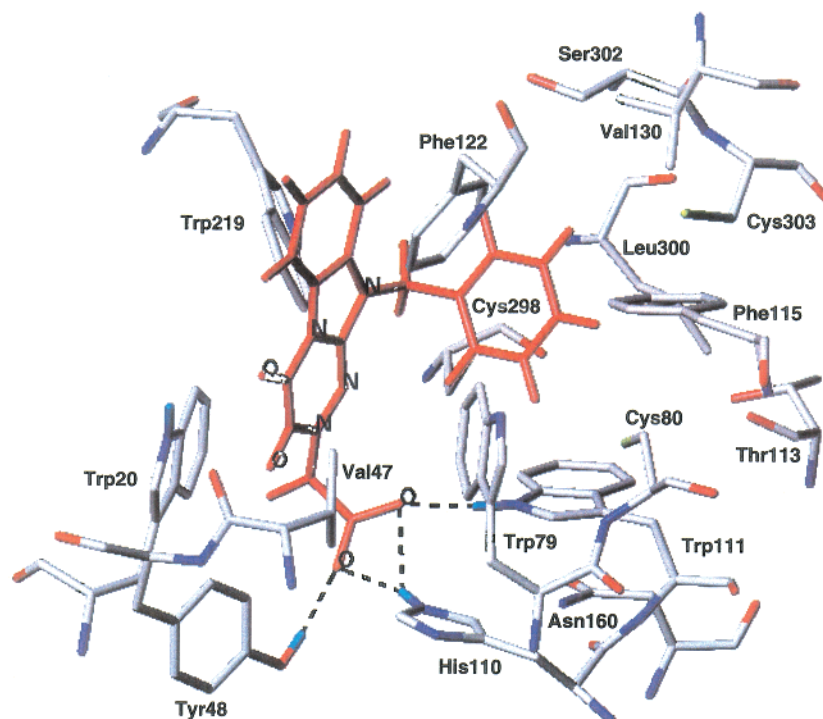


Figure 3. Compound **3** docked into the ALR2 active site. Only amino acids located within 5 Å of the inhibitor are displayed for the sake of clarity.

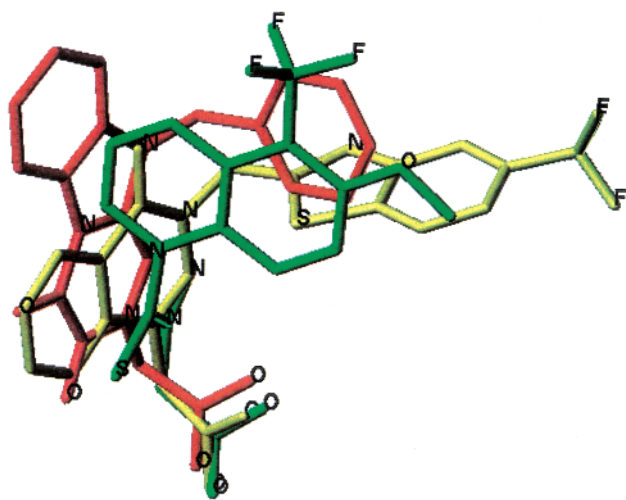


Figure 4. Overlay of the putative bioactive conformation of **3** (red) on the experimentally determined ALR2-bound conformations of zopolrestat (yellow) and tolrestat (green).

products are reported in Table 1. Spectral data for **38**, which is representative of the title compounds, are listed below.

1-Methyl-2-hydrazinobenzimidazole, 38. IR, ν cm^{-1} : 3320, 3225, 1550, 720. ^1H NMR, δ : 3.48 (s, 3H, CH_3), 6.91–7.30 (m, 4H, ArH). MS, m/e : 162 [M^+], base.

General Procedure for the Synthesis of 10-Alkyl[1,2,4]-triazino[4,3-*a*]benzimidazol-3,4(10*H*)-diones 49–58. A solution of the appropriate 1-alkyl-2-hydrazinobenzimidazole (**38**–**47**, 1 mmol) and diethyl oxalate (0.16 mL, 1.2 mmol) in 5 mL of absolute ethanol was heated under reflux until the disappearance of the starting material (3–20 h, TLC analysis). After the mixture was cooled, a yellow solid separated, which was collected and recrystallized. Yields, recrystallization solvents, and melting points of the products are reported in Table 2. Spectral data for **49**, which is representative of the title compounds, are listed below.

10-Methyl[1,2,4]triazino[4,3-*a*]benzimidazol-3,4(10*H*)-dione, 49. IR, ν cm^{-1} : 3150, 1700, 1625, 1450. ^1H NMR, δ :

3.44 (s, 3H, CH_3), 7.13–8.13 (m, 4H, ArH), 12.11 (s, 1H, NH, exch with D_2O). MS, m/e : 216 [M^+], 131, base.

General Procedure for the Synthesis of Ethyl (10-Alkyl[1,2,4]triazino[4,3-*a*]benzimidazol-3,4(10*H*)-dion-2-yl)acetates 59–69. A suspension of **48**–**58** (1 mmol), ethyl bromoacetate (0.13 mL, 1.2 mmol), and anhydrous potassium carbonate (0.166 g, 1.2 mmol) in 5 mL of acetone was heated under reflux until the disappearance of the starting material (7–24 h, TLC analysis). After the mixture was cooled, the solid precipitate was collected, washed with water to remove the inorganic salts, and recrystallized. Yields, recrystallization solvents, and melting points of the products are reported in Table 3. Spectral data for **59**, which is representative of the title compounds, are listed below.

Ethyl (10-Methyl[1,2,4]triazino[4,3-*a*]benzimidazol-3,4(10*H*)-dion-2-yl)acetate, 59. IR, ν cm^{-1} : 1740, 1700, 1620, 1200. ^1H NMR, δ : 1.23 (t, 3H, CH_2CH_3), 3.44 (s, 3H, CH_3), 4.17 (q, 2H, CH_2CH_3), 4.69 (s, 2H, NCH_2), 7.13–8.12 (m, 4H, ArH). MS, m/e : 302 [M^+], 201, base.

General Procedure for the Synthesis of (1-Alkyl-3-oxalo-1*H*,3*H*-benzimidazol-2-ylidenehydrazino)acetic Acids 12–22. A suspension of the appropriate ester derivative (**59**–**69**, 1 mmol) in 3 mL of 3% NaOH was left under stirring at room temperature until a solution was achieved (1–48 h). The solution was then filtered and acidified with concentrated HCl under ice-cooling. The white solid precipitate was collected, washed with water, and recrystallized. Yields, recrystallization solvents, and cyclization temperatures to products **1**–**11** are reported in Table 4. Spectral data for **12**, which is representative of the title compounds, are listed below.

(1-Methyl-3-oxalo-1*H*,3*H*-benzimidazol-2-ylidenehydrazino)acetic Acid, 12. IR, ν cm^{-1} : 3250, 3150, 1710, 1600, 1580, 1260. ^1H NMR, δ : 3.78 (s, 3H, CH_3), 4.51 (s, 2H, CH_2), 7.39–7.63 (m, 4H, ArH). MS, m/e : 77, base.

General Procedure for the Synthesis of (10-Alkyl[1,2,4]triazino[4,3-*a*]benzimidazol-3,4(10*H*)-dion-2-yl)-acetic Acids 1–11. Method A. The dicarboxylic derivatives **12**–**22** (1 mmol) were heated at the appropriate temperature (see Table 4) until thermal cyclization occurred. Yields, recrystallization solvents, and melting points of the products are reported in Table 5.

Method B. A suspension of the ester derivative (**59–69**, 1 mmol) in 1 mL of concentrated HCl was heated, under stirring at 100 °C, until hydrolysis was complete (12–72 h, TLC analysis). After cooling, the reaction mixture was diluted with water and the yellow solid that precipitated was collected and recrystallized from the appropriate solvent. Spectral data for **1**, which is representative of the title compounds, are listed below.

(10-Methyl[1,2,4]triazino[4,3-*a*]benzimidazol-3,4(10*H*)-dion-2-yl)acetic Acid, **1.** IR, ν cm⁻¹: 3400, 1720, 1590, 1200, 900. ¹H NMR, δ : 3.45 (s, 3H, CH₃), 4.60 (s, 2H, CH₂), 7.16–8.12 (m, 4H, ArH). MS, m/e : 274 [M⁺], 77, base.

General Procedure for the Synthesis of Ethyl (10-Alkyl[1,2,4]triazino[4,3-*a*]benzimidazol-4(10*H*)-on-3-yl)-acetates **70–72.** A solution of the suitable 2-hydrazinobenzimidazole **37**, **38**, and **40** (1 mmol) and diethyl acetylenedicarboxylate (0.19 mL, 1.2 mmol) in 5 mL of methanol was heated under reflux until the disappearance of the starting material (8–48 h, TLC analysis). After the mixture was cooled, the yellow solid precipitate was collected and recrystallized. Yields, recrystallization solvents, and melting points of the products are reported in Table 6. Spectral data for **72**, which is representative of the title compounds, are listed below.

Ethyl (10-Benzyl[1,2,4]triazino[4,3-*a*]benzimidazol-4(10*H*)-on-3-yl)acetate, **72.** IR, ν cm⁻¹: 1720, 1660, 1560. ¹H NMR, δ : 1.19 (t, 3H, CH₂CH₃), 3.98 (s, 2H, CH₂), 4.11 (q, 2H, CH₂CH₃), 5.18 (s, 2H, CH₂Ar), 7.37–8.41 (m, 9H, ArH). MS, m/e : 362 [M⁺], 91, base.

General Procedure for the Synthesis of (10-Alkyl[1,2,4]triazino[4,3-*a*]benzimidazol-4(10*H*)-on-3-yl)acetic Acids **23–25.** A suspension of the appropriate ester derivative (**70–72**, 1 mmol) in 1 mL of concentrated HCl was heated under stirring at 100 °C until hydrolysis was complete (2–4 h, TLC analysis). After cooling, the reaction mixture was diluted with water and the solid precipitate was collected and recrystallized. Yields, recrystallization solvents, and melting points of the products are reported in Table 6. Spectral data for **24**, which is representative of the title compounds, are listed below.

(10-Methyl[1,2,4]triazino[4,3-*a*]benzimidazol-4(10*H*)-on-3-yl)acetic Acid, **24.** IR, ν cm⁻¹: 1650, 1640, 1550. ¹H NMR, δ : 3.83 (s, 3H, CH₃), 3.86 (s, 2H, CH₂), 7.30–8.37 (m, 4H, ArH). MS, m/e : 118, base.

***i*-Propyl (10-Benzyl[1,2,4]triazino[4,3-*a*]benzimidazol-3,4(10*H*)-dion-2-yl)acetate, **73**.** Compound **73** was obtained following a procedure analogous to that employed for the preparation of compounds **59–69** using *i*-propyl bromoacetate instead of ethyl bromoacetate. After recrystallization from *i*-propyl alcohol, pure **73** was obtained with a 61% yield. Mp: 246–247 °C. IR, ν cm⁻¹: 1740, 1700, 1600, 1180. ¹H NMR, δ : 1.17 (s, 3H, CH₃), 1.25 (s, 3H, CH₃), 3.09 (m, 1H, CH), 4.66 (s, 2H, NCH₂), 5.17 (s, 2H, CH₂Ar), 7.33–8.18 (m, 9H, ArH). MS, m/e : 392 [M⁺], 91, base. Anal. Calcd for C₂₁H₂₀N₄O₄.

2. Biology. 2.1. Materials and Methods. Aldose reductase (ALR2) and aldehyde reductase (ALR1) were obtained from Sprague Dawley albino rats, 120–140 g body weight, supplied by Harlan Nossan, Italy. In order to minimize cross-contamination between ALR2 and ALR1 in the enzyme preparation, rat lens, in which ALR2 is the predominant enzyme, and kidney, where ALR1 shows the highest concentration, were used for isolation of ALR2 and ALR1, respectively.

Glutathione reductase (GR) type IV from baker's yeast (100–300 U/mg), sorbitol dehydrogenase (SD) from sheep liver (10 U/mg of protein), pyridine coenzymes, D,L-glyceraldehyde, glutathione disulfide, sodium D-glucuronate, sorbitol, and quercetin were from Sigma Chemical Co. Sorbinil was a gift from Pfizer, Groton, CT. Tolrestat was extracted from Lorestat Recordati, Italy. All other chemicals were of reagent grade.

2.2. Enzyme Preparation. 2.2.1. Aldose Reductase (ALR2). A purified rat lens extract was prepared in accordance with the method of Hayman and Kinoshita⁴⁷ with slight modifications. Lenses were quickly removed from normal killed rats and homogenized (Glas-Potter) in three volumes of cold,

deionized water. The homogenate was centrifuged at 12 000 rpm at 0–4 °C for 30 min. Saturated ammonium sulfate solution was added to the supernatant fraction to form a 40% solution, which was stirred for 30 min at 0–4 °C and then centrifuged at 12 000 rpm for 15 min. Following this same procedure, the recovered supernatant was subsequently fractionated with saturated ammonium sulfate solution, using first a 50% and then a 75% of salt saturation. The precipitate recovered from the 75% saturated fraction, containing ALR2 activity, was redissolved in 0.05 M NaCl and dialyzed overnight in 0.05 M NaCl. The dialyzed material was used for the enzymatic assay.

2.2.2. Aldehyde Reductase (ALR1). Rat kidney ALR1 was prepared in accordance with a previously reported method.²⁶ Kidneys were quickly removed from normal killed rats and homogenized (Glas-Potter) in three volumes of 10 mM sodium phosphate buffer, pH = 7.2, containing 0.25 M sucrose, 2.0 mM EDTA dipotassium salt, and 2.5 mM β -mercaptoethanol. The homogenate was centrifuged at 12 000 rpm at 0–4 °C for 30 min, and the supernatant was subjected to a 40–75% ammonium sulfate fractionation, following the same procedure previously described for ALR2. The precipitate obtained from the 75% ammonium sulfate saturation, containing ALR1 activity, was redissolved in 50 volumes of 10 mM sodium phosphate buffer, pH = 7.2, containing 2.0 mM EDTA dipotassium salt and 2.0 mM β -mercaptoethanol and dialyzed overnight using the same buffer. The dialyzed material was used in the enzymatic assay.

2.3. Enzymatic Assays. The activity of the four test enzymes was determined spectrophotometrically by monitoring the change in absorbance at 340 nm, which is due to the oxidation of NADPH or the reduction of NAD⁺ catalyzed by ALR2, ALR1, and GR or SD, respectively. The change in pyridine coenzyme concentration per minute was determined using a Beckman DU-64 kinetics software program (Solf Pack TM module).

ALR2 activity was assayed at 30 °C in a reaction mixture containing 0.25 mL of 10 mM D,L-glyceraldehyde, 0.25 mL of 0.104 mM NADPH, 0.25 mL of 0.1 M sodium phosphate buffer (pH = 6.2), 0.1 mL of enzyme extract, and 0.15 mL of deionized water in a total volume of 1 mL. All the above reagents, except D,L-glyceraldehyde, were incubated at 30 °C for 10 min; the substrate was then added to start the reaction, which was monitored for 5 min. Enzyme activity was calibrated by diluting the enzymatic solution in order to obtain an average reaction rate of 0.011 \pm 0.0010 AU/min for the sample.

ALR1 activity was determined at 37 °C in a reaction mixture containing 0.25 mL of 20 mM sodium D-glucuronate, 0.25 mL of 0.12 mM NADPH, 0.25 mL of dialyzed enzymatic solution, and 0.25 mL of 0.1 M sodium phosphate buffer (pH = 7.2) in a total volume of 1 mL. The enzyme activity was calibrated by diluting the dialyzed enzymatic solution in order to obtain an average reaction rate of 0.015 \pm 0.0010 AU/min for the sample.

SD activity²⁵ was determined at 37 °C in a reaction mixture containing 0.25 mL of 10 mM sorbitol, 0.25 mL of 0.47 mM NAD⁺, 0.25 mL of 3.75 mU/mL enzymatic solution, 0.25 mL of 100 mM Tris-HCl buffer (pH = 8) in a total volume of 1 mL. All the reagents were incubated at 37 °C for 1 min, after which the reaction was monitored for 3 min.

GR activity²⁷ was determined at 37 °C in a mixture containing 0.25 mL of 1 mM glutathione disulfide, 0.25 mL of 0.36 mM NADPH, 0.25 mL of 4.5 mU/mL enzymatic solution, 0.25 mL of 0.125 sodium phosphate buffer (pH = 7.4) supplemented with 6.3 mM EDTA potassium salt, in a total volume of 1 mL.

2.4. Enzymatic Inhibition. The inhibitory activity of the newly synthesized compounds against ALR2, ALR1, SD, and GR was assayed by adding 0.1 mL of the inhibitor solution to the reaction mixture described above. All the inhibitors were dissolved in water, and the solubility was facilitated by adjustment to a favorable pH. After complete dissolution, the pH was readjusted to 7. To correct for the nonenzymatic oxidation of NADPH or reduction of NAD⁺ and for the

absorption by the compounds tested, a reference blank containing all the above assay components except the substrate was prepared. The inhibitory effect of the new derivatives was routinely estimated at a concentration of 10^{-5} M. Those compounds found to be active were tested at additional concentrations between 10^{-5} and 10^{-8} M. The determination of the IC_{50} values was performed by using linear regression analysis of the log of the dose-response curve, which was generated using at least four concentrations of inhibitor, causing an inhibition between 20% and 80% with two replicates at each concentration. The 95% confidence limits (95% CL) were calculated from t values for $n - 2$, where n is the total number of determinations.

3. Pharmacology. 3.1. Materials and Methods. Experiments were carried out using Sprague Dawley albino rats, 45–55 g body weight, supplied by Harlan-Nossan, Italy. Animal care and treatment conformed to the ARVO resolution on the use of animals in ophthalmic and vision research. The galactose diet consisted of a pulverized mixture of 50% D-galactose and 50% TRM (Harlan Teckland, U.K.) and laboratory chow, and the control diet consisted of normal TRM. Both control and experimental rats had access to food and water ad libitum.

3.2. Prevention of Cataract Development. Animals were randomly divided into groups of equal average body weight with 15 rats per group. The test compounds **3**, **73**, and tolrestat were administered four times daily as eyedrops of appropriate concentrations. The vehicle in which ARIs were contained was administered with the same dose regimen to the control group, which was given access to the galactose diet, and to the group fed with normal diet, which was included to record the aspect of normal lenses. Groups treated with the tested compounds were predosed 1 day before switching their diet to galactose-containing chow.

Lenses were examined using slit-lamp microscopy, after dilating the pupils with 1% atropina, Farmigea, Italy, to establish their status of integrity.

Nuclear cataracts, which appeared as a pronounced central opacity readily visible as a white spot, were considered. The number of animals that attained this stage was recorded, and the ability of the test compounds to prevent cataract development was assessed on the basis of comparison with galactosemic rats treated only with the vehicle.

4. Computational Chemistry. Molecular modeling and graphics manipulations were performed using the SYBYL⁴⁸ and MIDAS⁴⁹ software packages, running them on a Silicon Graphics R10000 workstation. Model building and conformational analysis of compound **3** were accomplished with the TRIPOS force field⁵⁰ available within SYBYL. Point charges of this inhibitor were calculated using the semiempirical quantum mechanics AM1 method⁵¹ implemented in the MOPAC program.⁵² Energy minimizations and molecular dynamics simulations of the ALR2/NADP⁺ and ALR2/NADP⁺/**3** complexes were realized by employing the AMBER program,^{37,38} selecting the all-atom Cornell et al. force field.⁵³

4.1. Building a Model of Human ALR2. It is known from crystallographic^{6,7} and modeling studies^{11,54} that the binding of inhibitors to the ALR2 active site induces fairly significant conformational changes in a loop (residues 121–135) and a short segment (residues 298–303). These changes are associated with the opening of the so-called specificity pocket, which is completely closed in the absence of the inhibitor. The X-ray structure of the human ALR2/NADP⁺/zopolrestat complex has been published by Wilson et al.⁶ but could not be used in this modeling study because only the coordinates of the corresponding C α atoms are filed in the Brookhaven Protein Data Bank³⁵ (PDB entry code 1MAR). A model of human ALR2 was built starting from the crystal structures of the human ALR2 holoenzyme (PDB entry code 1ADS)³⁶ and the porcine ALR2/NADP⁺/tolrestat complex (PDB entry code 1AH3).⁷ A superposition of the proteins about their C α atoms yielded a root-mean-square (rms) deviation of 0.83 Å. Such a close structural similarity is not surprising because the two ALR2 isoforms share more than 84% sequence identity, the only differences being confined to the loop 121–135 and the segment 298–

303. The backbone of the above-listed residues in the human ALR2 holoenzyme (closed specificity pocket) was replaced with that of porcine ALR2/NADP⁺/tolrestat complex (open specificity pocket). All the nonidentical side chains were then mutated into those of the human type through the SYBYL/MUTATE command. The Asn129 side chain atoms, not included in the crystal structure of human ALR2 owing to disorder, were generated using the AMBER internal coordinate database. With the exception of His110, all His residues were treated as neutral species with the hydrogen assigned to the N^{δ1}. His110 was modeled in its N^{ε2} tautomeric form on the basis of the crystallographic evidence that the carboxylate group of zopolrestat is salt-linked to the N^{ε2} hydrogen of His110.^{9,55–57} Recent modeling studies of substrates in the ALR2 binding site suggest that His110 is not protonated.⁵⁸ Asp and Glu residues were assumed to be negatively charged, while Arg and Lys were positively charged. Hydrogen atoms were added to the protein through the SYBYL/BIOPOLYMER module.

To refine the resulting model, we adopted the following energy minimization protocol. Stretches 121–135 and 298–303 were locally minimized through 200 steps of steepest descent followed by 300 steps of conjugate gradient, while the rest of the system was kept fixed. Next, the whole protein was minimized in vacuo using a distance-dependent dielectric function ($\epsilon = 4r$) and constraining the position of the backbone atoms with a harmonic force constant of 10 kcal/mol Å². During this step, NADP⁺ was allowed to move. Energy minimizations were realized by setting a nonbonded cutoff of 8 Å and an energy gradient of 0.01 kcal/mol as the convergence criterion. In all AMBER calculations, the atomic charges for NADP⁺ were calculated by an electrostatic potential fit⁵⁹ to a STO-3G ab initio wave function.

4.2. Model Building and Conformational Analysis of Compound 3. A molecular model of compound **3** was constructed using standard bond lengths and bond angles of the SYBYL fragment library. The carboxylate group was taken as dissociated. Atom-centered partial charges were calculated using the AM1 Hamiltonian⁵¹ as implemented in MOPAC⁵² (CHARGE = -1; keywords, PREC, GNORM = 0.01, EF, MMOK). Geometry optimizations were realized with the SYBYL/MAXIMIN2 minimizer by applying the BFGS (Broyden, Fletcher, Goldfarb, and Shannon) algorithm⁶⁰ and setting an rms gradient of the forces acting on each atom of 0.05 kcal/mol Å as the convergence criterion.

Representative energetically stable conformations of **3** were sought for a pharmacophore-based superposition on the ALR2-bound conformation of zopolrestat, as well as for docking calculations. A conformational analysis on **3** was carried out using the SYBYL/SEARCH module. The torsional angles defined in Figure 2 were scanned by 20° increments throughout 0–340° (τ_2 and τ_3) or 0–160° (τ_1 and τ_4). A van der Waals scaling factor of 0.75 was applied to “soften” steric contacts to take into account the lack of relaxation in the rigid rotamers. The number of output conformations to be examined was reduced by setting the “energy window” (energy difference between the generated conformation and the current minimum) to 5.0 kcal/mol. The resulting conformations were classified in the grid space of torsional angles into 16 “families”, using the FAMILY option of the SYBYL/MOLECULAR SPREADSHEET routine.

The lowest energy conformation of each family was superimposed on the ALR2-bound geometry of zopolrestat⁶ by fitting the carboxylate carbons, the triazinobenzimidazole N1 and N10 on the phthalazine N2 and N3, respectively. The conformation of **3** affording the best overlay on zopolrestat (Figure 1) was defined by the following values of torsion angles: $\tau_1 = 135^\circ$, $\tau_2 = 106^\circ$, $\tau_3 = -115^\circ$, and $\tau_4 = 39^\circ$. Compound **25** was modeled and aligned on zopolrestat, following a similar procedure. The conformation of **25** illustrated in Figure 1 features the following values of torsion angles (defined analogously to those of **3**): $\tau_1 = 59^\circ$, $\tau_2 = 63^\circ$, $\tau_3 = -118^\circ$, and $\tau_4 = 44^\circ$.

4.3. Docking of Compound 3 into the ALR2 Active Site. Docking calculations were performed using the DOCK suite

of programs.^{40–43} DOCK describes the binding site of the target protein as a cluster of spheres filling the binding cavity to conform to its shape. Docking is achieved by treating the protein and the ligand as rigid entities and searching for matches between interatomic and intersphere distances. To take into account the flexibility of the ligand, a set of different geometries of the ligand, representative of its conformational chances, can be individually docked. Several binding modes are generated for each ligand conformation, with each receiving a score dictated by the steric and electrostatic energies calculated by a molecular mechanics force field.^{40–43}

The refined model of the ALR2/NADP⁺ complex, without hydrogen atoms, was used to create the solvent-accessible molecular surface in accordance with the Connolly algorithm.^{61,62} The program SPHGEN was used to generate spheres that fill the enzyme active site. The target area was covered by a manually edited cluster made up of 34 individual spheres. Each sphere was assigned a close contact limiting distance of 1.3 and 1.8 Å for the polar and nonpolar atoms, respectively. A cutoff distance of 4.5 Å for “good contacts” with the protein was used.^{61,62} The contact and force field grids generated using the DISTMAP and CHEMGRID modules in DOCK were used to score the different orientations of the ligand bound to the enzyme. DOCK was run in the SINGLE mode option by investigating all the possible binding orientations.

The reliability of DOCK and the validity of the assumptions concerning the modeled enzyme structure were confirmed by attempting the redocking of the crystal structures of zopolrestat and tolrestat. The most stable docking models identified by DOCK closely reproduced the two experimentally determined binding modes.

Each of the above representative 16 low-energy conformations of **3** was at this point docked into the ALR2 active site. Interestingly, the top scoring value was achieved by the conformation yielding the best overlay on the ALR2-bound conformation of zopolrestat (Figure 1). Out of the 1305 orientations of this conformation, 43 were within 5 kcal/mol of the best orientation based on the scoring function. Inspection of the docked structures revealed that the best and many of the top-scoring orientations placed the negatively charged carboxylate group of **3** into the anionic binding site of ALR2 lined by residues Tyr48, His110, and Trp111 to make a network of hydrogen bonds. From this cluster of structures, we selected one (the top-scoring one with a force field score of −43.6 kcal/mol) in which the benzyl group was located in the specificity pocket occupied by the benzothiazole moiety of zopolrestat in the crystal structure.

The parameters of **3** were set consistently with the Cornell et al. force field;⁵³ missing bond and angle parameters were assigned on the basis of analogy with known parameters in the database and calibrated to reproduce the AM1 optimized geometry. The complex was solvated by the addition of 217 TIP3P water molecules⁶³ within 20 Å of the inhibitor. The water molecules alone were minimized (20 000 cycles or 0.1 kcal/mol rms deviation in energy) and equilibrated for 5 ps in a constant temperature (300 K) bath. The entire system was then subjected to SANDER energy minimization (<0.01 kcal/mol rms deviation) followed by a 200 ps MD run. During the simulation the positional constraints on the protein backbone were gradually reduced from 5 to 0.1 kcal Å^{−2} mol^{−1}. The SHAKE option was used to constrain bonds involving hydrogen. A 1 fs time step was used along with a nonbonded cutoff of 8 Å at 1 atm of constant pressure. The temperature was maintained at 300 K using the Berendsen algorithm⁶⁴ with a coupling constant of 0.2 ps. Four snapshots, extracted every 25 ps from the last 100 ps MD simulation, proved to be very similar in terms of rms deviation. An average structure was calculated from the last 100 ps trajectory, and the energy was minimized using the steepest descent and conjugate gradient methods available within the SANDER module of AMBER.

References

- (1) Ammon, H. P. T.; Häring, H. U.; Kellerer, M.; Laube, H.; Mosthaf, L.; Verspohl, E. J.; Wahl, M. A. Antidiabetic Agents. Recent Advances in Their Molecular and Clinical Pharmacology. *Adv. Drug Res.* **1996**, *27*, 171–178.
- (2) Tomlinson, D. R.; Stevens, E. J.; Diemel, L. T. Aldose Reductase Inhibitors and Their Potential for the Treatment of Diabetic Complications. *Trends Pharmacol. Sci.* **1994**, 293–297.
- (3) Costantino, L.; Rastelli, G.; Vianello, P.; Cignarella, G.; Barlocco, D. Diabetes Complications and Their Potential Prevention: Aldose Reductase Inhibition and Other Approaches. *Med. Res. Rev.* **1999**, *19*, 3–23.
- (4) Kador, P. F. The Role of Aldose Reductase in the Development of Diabetic Complications. *Med. Res. Rev.* **1988**, *8*, 325–352.
- (5) Sarges, R.; Oates, P. J. Aldose Reductase Inhibitors: Recent Developments. *Prog. Drug Res.* **1993**, *40*, 99–161.
- (6) Wilson, D. K.; Tarle, I.; Petrash, J. M.; Quiocho, F. A. Refined 1.8 Å Structure of Human Aldose Reductase Complexed with the Potent Inhibitor Zopolrestat. *Proc. Natl. Acad. Sci. U.S.A.* **1993**, *90*, 9847–9851.
- (7) Urzhumtsev, A.; Tête-Favier, F.; Mitschler, A.; Barbant, J.; Barth, P.; Urzhumtseva, L.; Biellmann, J.-F.; Podjarny, A. D.; Moras, D. A “Specificity” Pocket Inferred from the Crystal Structures of the Complexes of Aldose Reductase with the Pharmacologically Important Inhibitors Tolrestat and Sorbinil. *Structure* **1997**, *5*, 601–612.
- (8) Harrison, D. H. T.; Bohren, K. M.; Petsko, G. A.; Ringe, D.; Gabbay, K. H. The Alrestatin Double-Decker: Binding of Two Inhibitor Molecules to Human Aldose Reductase Reveals a New Specificity Determinant. *Biochemistry* **1997**, *36*, 16134–16140.
- (9) Harrison, D. H.; Bohren, K. M.; Ringe, D.; Petsko, G. A.; Gabbay, K. H. An Anionic Binding Site in Human Aldose Reductase: Mechanistic Implications for the Binding of Citrate, Cadylate, and Glucose-6-phosphate. *Biochemistry* **1994**, *33*, 2011–2020.
- (10) Carper, D.; Wistow, G.; Nishimura, C.; Graham, C.; Watanabe, K.; Fujii, Y.; Hayaishi, H.; Hayaishi, O. A Superfamily of NADPH-Dependent Reductases in Eukaryotes and Prokaryotes. *Exp. Eye Res.* **1988**, *49*, 377–388.
- (11) Costantino, L.; Rastelli, G.; Vescovini, K.; Cignarella, G.; Vianello, P.; Del Corso, A.; Cappiello, M.; Mura, U.; Barlocco, D. Synthesis, Activity, and Molecular Modeling of a New Series of Tricyclic Pyridazinones as Selective Aldose Reductase Inhibitors. *J. Med. Chem.* **1996**, *39*, 4396–4405.
- (12) Giblin, F. J.; McCready, J. P.; Schirmscher, L.; Reddy, V. N. Peroxide-Induced Effects on Lens Cation Transport Following Inhibition of Glutathione Reductase Activity in Vitro. *Exp. Eye Res.* **1987**, *45*, 77–91.
- (13) Reddan, J. R.; Giblin, F. J.; Dziedzic, D. C.; McCready, J. P.; Schirmscher, L.; Reddy, V. N. Influence of the Activity of Glutathione Reductase on the Response of Cultured Lens Epithelial Cells from Young and Old Rabbits to Hydrogen Peroxide. *Exp. Eye Res.* **1998**, *46*, 209–221.
- (14) Masson, E. A.; Boulton, A. J. Aldose Reductase Inhibitors in the Treatment of Diabetic Neuropathy. A Review of the Rationale and Clinical Evidence. *Drugs* **1990**, *39*, 190–202.
- (15) Primofiore, G.; Da Settimo, F.; Taliani, S.; Marini, A. M.; La Motta, C.; Novellino, E.; Greco, G.; Gesi, M.; Trincavelli, L.; Martini, C. 3-Aryl[1,2,4]triazino[4,3-*a*]benzimidazol-4(10*H*)-ones: Tricyclic Heteroaromatic Derivatives as a New Class of Benzodiazepine Receptor Ligands. *J. Med. Chem.* **2000**, *43*, 96–102.
- (16) Da Settimo, F.; Primofiore, G.; Taliani, S.; Marini, A. M.; La Motta, C.; Novellino, E.; Greco, G.; Lavecchia, A.; Trincavelli, L.; Martini, C. 3-Aryl[1,2,4]triazino[4,3-*a*]benzimidazol-4(10*H*)-ones: A New Class of Selective A₁ Adenosine Receptor Antagonists. *J. Med. Chem.* **2001**, *44*, 316–339.
- (17) Tacconi, V. G.; Righetti, P. P.; Desimoni, G. Einfache Darstellung von N-Substituierten Isatinen (An Easy Synthesis of N-Substituted Isatins). *J. Prakt. Chem.* **1973**, *315*, 339–344.
- (18) Bednyagina, N. P.; Postovskii, I. Ya. Benzazoles. 2-Hydrazino- and 2-Azidobenzimidazoles. *Zh. Obshch. Khim.* **1960**, *30*, 1431–1437; *Chem. Abstr.* **1961**, *55*, 1586h.
- (19) Badr, M. Z. A.; Mahmoud, A. M.; Mahgoub, S. A.; Hozien, Z. A. Condensation and Cyclization Reactions of 2-Hydrazinobenzimidazole, -benzoxazole, and -benzothiazole. *Bull. Chem. Soc. Jpn.* **1988**, *61*, 1339–1344.
- (20) Le Count, D. J.; Greer, A. T. Cyclization of Heterocyclic Hydrazones Prepared from Dimethyl Acetylenedicarboxylate. *J. Chem. Soc., Perkin Trans. 1* **1974**, 297–301.
- (21) De Ruiter, J.; Brubaker, A. N.; Garner, M. A.; Barksdale, J. M.; Mayfield, C. A. In Vitro Aldose Reductase Inhibitory Activity of Substituted N-Benzenesulfonylglycine Derivatives. *J. Pharm. Sci.* **1987**, *76*, 149–152.
- (22) Mayfield, C. A.; De Ruiter, J. Novel Inhibitors of Rat Lens Aldose Reductase: N-[(Substituted amino)phenyl]sulfonylglycines. *J. Med. Chem.* **1987**, *30*, 1595–1598.

- (23) Müller, P.; Hockwin, O.; Ohrloff, C. Comparison of Aldose Reductase Inhibitors by Determination of IC₅₀ with Bovine and Rat Lens Extracts. *Ophthalmic Res.* **1985**, *17*, 115–119.
- (24) Hockwin, O.; Müller, P.; Krolczyk, J.; McCue, B. A.; Mayer, P. R. Determination of AL01576 Concentration in Rat Lenses and Plasma by Bioassay for Aldose Reductase Activity Measurements. *Ophthalmic Res.* **1989**, *21*, 285–291.
- (25) Lindstad, R. I.; Hermansen, L. F.; McKinley-McKee, J. S. Inhibition and Activation Studies on Sheep Liver Sorbitol Dehydrogenase. *Eur. J. Biochem.* **1994**, *221*, 847–854.
- (26) Ward, W. H. J.; Sennitt, C. M.; Ross, H.; Dingle, A.; Timmus, D.; Mirrless, D. J.; Tuffin, D. P. Ponalrestat, a Potent and Specific Inhibitor of Aldose Reductase. *Biochem. Pharmacol.* **1990**, *39*, 337–346.
- (27) Fitzgerald, G. B.; Bauman, C.; Sajjat Hussoin, Md.; Wick, M. M. 2,4-Dihydroxy benzylamine: A Specific Inhibitor of Glutathione Reductase. *Biochem. Pharmacol.* **1991**, *41*, 185–190.
- (28) Hu, T.; Merola, L. O.; Kuwabara, T.; Kinoshita, J. H. Prevention and Reversal of Galactose Cataract in Rats with Topical Sorbinil. *Invest. Ophthalmol. Visual Sci.* **1984**, *25*, 603–605.
- (29) Sestan, K.; Bellini, F.; Fung, S.; Abraham, N.; Treasurywala, A.; Humber, L.; Simard-Duquesne, N.; Dvornik, D. N-[5-(Trifluoromethyl)-6-methoxy-1-naphthalenyl]thioxomethyl]-N-methylglycine (Tolrestat), a Potent, Orally Active Aldose Reductase Inhibitor. *J. Med. Chem.* **1984**, *27*, 255–256.
- (30) Banditelli, S.; Boldrini, E.; Vilardo, G. P.; Ceconi, I.; Cappiello, M.; Dal Monte, M.; Marini, I.; Del Corso, A.; Mura, U. A New Approach Against Sugar Cataract Through Aldose Reductase Inhibitors. *Exp. Eye Res.* **1999**, *69*, 533–538.
- (31) Chaudhry, P. S.; Cabrera, J.; Juliani, H. R.; Varma, S. D. Inhibition of Human Lens Aldose Reductase by Flavonoids, Sulindac and Indomethacin. *Biochem. Pharmacol.* **1983**, *32*, 1995–1998.
- (32) Camber, O.; Edman, P. Factors Influencing the Corneal Permeability of Prostaglandin F_{2α} and Its Isopropyl Ester in Vitro. *Int. J. Pharm.* **1987**, *37*, 27–32.
- (33) Suhonen, P.; Järvinen, T.; Peura, P.; Urtti, A. Permeability of Polycyclic Acid Diesters Across Albino Rabbit Cornea in Vitro. *Int. J. Pharm.* **1991**, *74*, 221–228.
- (34) Chien, D.-S.; Tang-Liu, D. D.-S.; Woodward, D. F. Ocular Penetration and Bioconversion of Prostaglandin F_{2α} Prodrugs in Rabbit Cornea and Conjunctiva. *J. Pharm. Sci.* **1997**, *86*, 1180–1186.
- (35) Bernstein, F. C.; Koetzle, T. F.; Williams, G. J. B.; Meyer, E. F., Jr.; Brice, M. D.; Rodgers, J. R.; Kennard, O.; Shimanouchi, T.; Tasumi, T. The Protein Data Bank: A Computer Based Archival File for Macromolecular Structures. *J. Mol. Biol.* **1977**, *112*, 535–542.
- (36) Wilson, D. K.; Bohren, K. M.; Gabbay, K. H.; Quijcho, F. A. An Unlikely Sugar Substrate Site in the 1.65 Å Structure of the Human Aldose Reductase Holoenzyme Implicated in Diabetic Complications. *Science* **1992**, *257*, 81–84.
- (37) Pearlman, D. A.; Case, D. A.; Caldwell, J. W.; Ross, W. S.; Cheatham, T. E., III; Debolt, S.; Ferguson, D. M.; Seibel, G. L.; Kollman, P. A. AMBER, a Package of Computer Programs for Applying Molecular Mechanics, Normal Mode Analysis, Molecular Dynamics and Free Energy Calculations To Simulate the Structural and Energetic Properties of Molecules. *Comput. Phys. Commun.* **1995**, *91*, 1–41.
- (38) Pearlman, D. A.; Case, D. A.; Caldwell, J. W.; Ross, W. S.; Cheatham, T. E., III; Ferguson, D. M.; Seibel, G.; Singh, U. C.; Weiner, P. K.; Kollman, P. A. AMBER, version 4.1; Department of Pharmaceutical Chemistry, University of California: San Francisco, CA, 1995.
- (39) Database searching (SWISS-PROT), sequence alignment, and analysis of rat and human ALR2 sequences were carried out using FASTA (Pearson, W. R. *Proc. Natl. Acad. Sci. U.S.A.* **1988**, *85*, 2444–2448) and BLAST programs (Pak, Y.; Wang, S. *J. Phys. Chem. B* **2000**, *104*, 354–359). The SWISS-PROT accession numbers for rat and human ALR2 types are P07943 and P15121, respectively.
- (40) Meng, E. C.; Shoichet, B. K.; Kuntz, I. D. Automated Docking with Grid-Based Energy Evaluation. *J. Comput. Chem.* **1992**, *13*, 505–524.
- (41) Meng, E. C.; Gschwend, D. A.; Blaney, J. M.; Kuntz, I. D. Orientational Sampling and Rigid-Body Minimization in Molecular Docking. *Proteins: Struct., Funct., Genet.* **1993**, *17*, 266–278.
- (42) Shoichet, B. K.; Bodian, D. L.; Kuntz, I. D. Molecular Modeling Using Shape Descriptors. *J. Comput. Chem.* **1992**, *13*, 380–397.
- (43) Connolly, M.; Gschwend, D. A.; Good, A. C.; Oshiro, C.; Kuntz, I. D. DOCK, version 3.5; Department of Pharmaceutical Chemistry University of California: San Francisco, CA, 1995.
- (44) Iemura, R.; Kawashima, T.; Fukuda, T.; Ito, K.; Tsukamoto, G. Synthesis of 2-(4-Substituted-1-piperazinyl)benzimidazoles as H₁-Antihistaminic Agents. *J. Med. Chem.* **1986**, *29*, 1178–1183.
- (45) Caroti, P.; Ceccotti, C.; Da Settimo, F.; Primofiore, G.; Franzone, J. S.; Reboani, M. C.; Cravanzola, C. Synthesis, Antilipidemic and Platelet Antiaggregatory Activity of 2-Aminobenzimidazole Amide Derivatives. *Farmacol.* **1989**, *44*, 227–255.
- (46) Anaya de Parodi, C.; Quintero-Cortes, L.; Sandoval-Ramirez, J. A Short Synthesis of Astemizole. *Synth. Commun.* **1996**, *26*, 3323–3330.
- (47) Hayman, S.; Kinoshita, J. H. Isolation and Properties of Lens Aldose Reductase. *J. Biol. Chem.* **1965**, *240*, 877–882.
- (48) SYBYL Molecular Modelling System, version 6.2; Tripos Inc.: St. Louis, MO, 1998.
- (49) Ferrin, T. E.; Huang, C. C.; Jarvis, L. E.; Langridge, R. The MIDAS Display System. *J. Mol. Graphics* **1998**, *6*, 13–27.
- (50) Vinter, J. G.; Davis, A.; Saunders, M. R. Strategic Approaches to Drug Design. 1. An Integrated Software Framework for Molecular Modelling. *J. Comput. Aided Mol. Des.* **1987**, *1*, 31–55.
- (51) Dewar, M. J. S.; Zoebisch, E. G.; Healy, E. F.; Stewart, J. J. P. AM1: A New General Purpose Mechanical Molecular Model. *J. Am. Chem. Soc.* **1985**, *107*, 3902–3909.
- (52) MOPAC (version 6.0) is available from Quantum Chemistry Program Exchange, No. 455.
- (53) Cornell, W. D.; Cieplak, P.; Bayly, C. I.; Gould, I. R.; Merz, K. M.; Ferguson, D. M.; Spellmeyer, D. C.; Fox, T.; Caldwell, J. W.; Kollman, P. A. A Second Generation Force Field for the Simulation of Proteins, Nucleic Acids, and Organic Molecules. *J. Am. Chem. Soc.* **1995**, *117*, 5179–5197.
- (54) Rastelli, G.; Costantino, L. Molecular Dynamics Simulations of the Structure of Aldose Reductase Complexed with the Inhibitor Tolrestat. *Bioorg. Med. Chem. Lett.* **1998**, *8*, 641–646.
- (55) Bohren, K. M.; Grimshaw, C. E.; Lai, C. J.; Harrison, D. H.; Ringe, D.; Petsko, G. A.; Gabbay, K. H. Tyrosine-48 is the Proton Donor and Histidine-110 Directs Substrate Stereochemical Selectivity in the Reduction Reaction of Human Aldose Reductase: Enzyme Kinetics and Crystal Structure of the Y48H Mutant Enzyme. *Biochemistry* **1994**, *33*, 2021–2032.
- (56) Petrash, J. M.; Hodosh, M.; Brooks, B. R.; Kador, P. F. Catalytic Mechanism of Aldose Reductase Studied by the Combined Potentials of Quantum Mechanics and Molecular Mechanics. *Biophys. Chem.* **1998**, *70*, 203–216.
- (57) Ehrig, T.; Bohren, K. M.; Prendergast, F. G.; Gabbay, K. H. Mechanism of Aldose Reductase Inhibition: Binding of NADP⁺/NADPH and Alrestatin-like Inhibitors. *Biochemistry* **1994**, *33*, 7157–7165.
- (58) De Winter, H. L.; von Itzstein, M. Aldose Reductase as a Target for Drug Design: Molecular Modeling Calculations on the Binding of Acyclic Sugar Substrates to the Enzyme. *Biochemistry* **1995**, *34*, 8299–8308.
- (59) Singh, U. C.; Kollmann, P. A. An Approach to Computing Electrostatic Charges for Molecules. *J. Comput. Chem.* **1984**, *5*, 129–144.
- (60) Head, J.; Zerner, M. C. A Broyden–Fletcher–Goldfarb–Shanno Optimization Procedure for Molecular Geometries. *Chem. Phys. Lett.* **1985**, *122*, 264–274.
- (61) Connolly, M. L. Solvent-Accessible Surfaces of Proteins and Nucleic Acids. *Science* **1983**, *221*, 709–713.
- (62) Connolly, M. L. Analytical Molecular Surface Calculation. *J. Appl. Crystallogr.* **1983**, *16*, 548–558.
- (63) Jorgensen, W. L.; Chandrasekhar, J.; Madura, J. D.; Impey, R. W.; Klein, M. L. Comparison of Simple Potential Functions for Simulating Liquid Water. *J. Chem. Phys.* **1983**, *79*, 926–935.
- (64) Berendsen, H. J. C.; Postma, J. P. M.; van Gunsteren, W. F.; DiNola, A.; Haak, J. R. Molecular Dynamics with Coupling to an External Bath. *J. Chem. Phys.* **1984**, *81*, 3684–3690.

JM0109210